

PAPER • OPEN ACCESS

A VMD-PE-SG denoising method based on K–L divergence for satellite atomic clock


To cite this article: Liang Yifeng *et al* 2023 *Meas. Sci. Technol.* **34** 055012

View the [article online](#) for updates and enhancements.

You may also like

- [New procedure to estimate plasma parameters through the q-Weibull distribution by using a Langmuir probe in a cold plasma](#)
F J Gonzalez, J I Gonzalez, S Soler et al.
- [The fractional Kullback–Leibler divergence](#)
A Alexopoulos
- [Improving the accuracy and sensitivity of ¹³C online detection in expiratory air using the TDLAS method in the spectral range of 4860–4880 cm⁻¹](#)
S V Kireev, A A Kondrashov and S L Shnyrev

A VMD-PE-SG denoising method based on K–L divergence for satellite atomic clock

Liang Yifeng , Xu Jiangning, Li Fangneng and Wu Miao*

College of Electrical Engineering, Naval University of Engineering, Wuhan, People's Republic of China

E-mail: wumiao9387@163.com

Received 11 July 2022, revised 28 October 2022

Accepted for publication 3 January 2023

Published 15 February 2023



CrossMark

Abstract

The time scale of the global navigation satellite system (GNSS) is the core element for its position, navigation and timing services. A highly stable atomic clock is essential to ensure the reliability of the GNSS time scale. This study proposed a novel hybrid denoising model combining variational mode decomposition (VMD), K–L divergence, permutation entropy (PE), and Savitzky–Golay (SG) filter for satellite atomic clocks. Firstly, the key parameter of VMD is solved efficiently by taking the minimum sum of K–L divergence of decomposed modes as the constraint condition, and the optimised parameters are applied to the decomposition process. On this basis, the PE algorithm is used to determine the modes decomposed by VMD into signal-dominant and noise-dominant components by searching for the mutation of PE value at two adjacent points. Finally, the noise-dominant components are denoised by the SG filter and then reconstructed with the signal-dominant components to form the denoised signal. The analysis of the simulated signal shows that the method can effectively remove noise from the simulated signal, and the resulting denoised signal is similar to the pure signal. Compared with commonly used ensemble empirical mode decomposition and wavelet denoising methods, the signal-noise ratio of the proposed method is improved by 21.2% and 28.9%, and the root mean square error is improved by 24.1% and 29.8%, respectively. The results of experimental data testify that the K–L VMD-PE-SG-based denoising method can significantly reduce the dominant noise within one day, thus effectively improving the short to medium-term frequency stability. Compared with the original signal, the stability of the smoothing time within 76 800 s is generally improved, and the degree of improvement depends on the type of atomic clock and the smoothing time.

Keywords: denoising, VMD, GNSS, satellite atomic clock, frequency stability, PE

(Some figures may appear in colour only in the online journal)

* Author to whom any correspondence should be addressed.



Original content from this work may be used under the terms of the [Creative Commons Attribution 4.0 licence](https://creativecommons.org/licenses/by/4.0/). Any further distribution of this work must maintain attribution to the author(s) and the title of the work, journal citation and DOI.

1. Introduction

Global navigation satellite system (GNSS) is a high-precision time synchronization system that requires a stable time scale along with high-precision atomic clock technology to realise navigation and time services [1]. However, because satellite atomic clocks operate in a complex environment, their signals often contain trend, multiple periodic and noise components. Among them, irregular noise is the main factor acting on the stability of an atomic clock, which would affect the extraction of the periodic term of a satellite atomic clock and would ultimately be detrimental to the generation and maintenance of a GNSS time scale [2]. Therefore, many signal-processing techniques have been applied to the data analysis of satellite atomic clocks, focusing on noise processing [3, 4].

In the common methods, the wavelet transform could be used to visualize signals in the time and frequency domain even with non-stationary signals, but these methods assume a stable signal exists in the wavelet window, and the choice of the wavelet basis is difficult to determine [5]. Kalman filtering has been widely used in clock signal denoising and state estimation, but it is still challenging to decompose the signal intuitively with a complex mathematical model [6]. Therefore, the empirical mode decomposition (EMD) proposed by Dr Huang and its derivative model have been gradually applied to atomic clock signal processing [5]. Zhu used ensemble empirical mode decomposition (EEMD) to denoise the frequency data of an atomic clock and achieved better denoising results than wavelet methods did [7]. Song used wavelet multiscale threshold denoising, thus achieving a stable time scale [8]. Mostafa used EMD to extract the stochastic components and successively improved the short-term stability of individual clocks and time scales [9]. However, EMD and its improved methods involve recursive mode decomposition, and their errors will gradually accumulate during the decomposition process. Many scholars have made improvements but failed to fundamentally solve the problems of pattern confusion and the effects on the endpoint [10, 11].

Dragomiretskiy and Zosso proposed the concept of variational mode decomposition (VMD) in 2014, transforming the signal decomposition into an optimization problem for constrained models by introducing a variational model to avoid endpoint effects, suppressing modal confusion and achieving higher decomposition efficiency [12]. It should be noted that VMD is obviously affected by the number of decompositions K and the penalty factor α . Optimization of the main parameters of VMD by use of a genetic algorithm and particle swarm optimization has been proposed in some studies, but processing time series with hundreds of points usually takes more than half an hour, which is difficult to accept in satellite navigation with high requirements for real-time [13, 14]. In addition, when using VMD, the first mode was often taken simply as the reconstructed signal. Thus the useful information contained in the other components would be ignored [15, 16].

In order to effectively denoise a satellite atomic clock signal and realise high-frequency stability, this study proposes a K–L VMD-Permutation entropy-Savitzky–Golay filter (K–L VMD-PE-SG)-based denoising method. The fast

parameter optimization of VMD parameters is realised by taking the minimum sum of K–L divergence of decomposed modes as the constraint condition. The paper introduced the PE algorithm to identify the mode obtained by VMD by determining the noise and signal components. The noise-dominated part was denoised by the SG filter method and then accumulated with the signal-dominated part to realise signal reconstruction. The simulated signal and experimental data of a GNSS atomic clock were analysed, respectively, and the effectiveness and practicability were verified by comparison with the EEMD and wavelet denoising methods.

The remainder of this study is arranged as follows. Section 2 introduces the model and noise characteristic of the satellite atomic clock and analyses the possible impact of noise components. Section 3 introduces the theoretical background, while section 4 focuses on describing the proposed K–L VMD-PE-SG-based data denoising method in this paper. In addition, section 5 applies the simulation signal the proposed method for decomposition and noise reduction and compared with the EEMD and wavelet denoising methods. After that, in section 6, based on the measured data of the BeiDou (BDS) and global navigation satellite system (GLONASS) satellite atomic clocks, the effectiveness of the proposed method is proved. Ultimately, section 7 gives the conclusion of this study.

2. Satellite atomic clock model and characteristic

The atomic clock model usually contains three parameters [17]:

- Initial clock offset a_0 , which represents the clock difference at time t_0 ;
- Initial frequency offset a_1 , which represents the relative frequency deviation at time t_0 ;
- The frequency drift a_2 , which represents the linear change of relative frequency deviation.

An atomic clock system can be considered as a numerical integrator that requires the three parameters mentioned above to form the oscillator. In terms of self-characterization and influence of the working environment, the stochastic differential equation of a satellite atomic clock could be generally expressed as:

$$\Delta t(t) = a_0 + a_1 t + \frac{1}{2} a_2 t^2 + \frac{A}{2\pi f_0} \sin(2\pi f_0 t + \varphi) \Big|_0^t + \sigma_1 W_1(t) + \sigma_2 \int_0^t W_2(s) ds + \sigma \varepsilon(t) \quad (1)$$

where a_0, a_1, a_2 could be regarded as constant values in a short period; $\frac{A}{2\pi f_0} \sin(2\pi f_0 t + \varphi) \Big|_0^t$ expressed the periodic component in the phase caused by the orbital motion of the satellites, which is usually bound by certain rules, especially for the main cycles; two independent Vener processes $W_1(t), W_2(t)$ usually represent white frequency modulation (WFM) noise and random walk frequency modulation noise (RWFM), respectively, and their corresponding diffusion coefficients of σ_1 and σ_2 are

used to represent the noise intensity; $\sigma\varepsilon(t)$ is the observation noise.

In the time domain, the square root of Allan variance, that is, Allan deviation (ADEV), is commonly used to characterize the frequency stability. The relationship between diffusion coefficients and Allan variance has been derived in [17]:

$$\sigma_y^2(\tau) = \sigma_1^2/\tau + \frac{1}{2}\sigma_2^2\tau \quad (2)$$

where $\sigma_y^2(\tau)$ represents the value of Allan variance when the smoothing time is τ . Correspondingly, the relationship between white phase modulation (WPM) noise, frequency drift, the period term and Allan variance could be derived in turn as follows [18–20]:

$$\sigma_y^2(\tau) = 3\sigma^2\tau^2 \quad (3)$$

$$\sigma_y^2(\tau) = \frac{1}{2}d^2\tau^2 \quad (4)$$

$$\sigma_y^2(\tau) = A^2 \frac{\sin^4(\pi f_0 \tau)}{(\pi f_0 \tau)^2}. \quad (5)$$

Combining the above factors, the Allan variance of the time deviation shown in formula (1) could be expressed as:

$$\sigma_y^2(\tau) = 3\sigma^2/\tau^2 + \sigma_1^2/\tau + \frac{1}{2}\sigma_2^2\tau + \frac{1}{2}d^2\tau^2 + A^2 \frac{\sin^4(\pi f_0 \tau)}{(\pi f_0 \tau)^2} \quad (6)$$

where the first term on the right of formula (6) is WPM, the second term is WFM, and both are the main factors affecting short-term stability, with slopes of -2 and -1 , respectively. The third term is RWFM, and the fourth term is frequency drift, which would mainly affect the atomic clock's long-term stability with a slow process of change. As the periodic fluctuation, the fifth term would cause the stability curve to bulge in a certain period. The first two relatively large factors would reduce a of a clock's short-term stability, an incorrect judgment of periodic items and an inaccurate satellite time scale. Therefore, the noise of an atomic clock should be eliminated, and the point is the frequency signal.

3. Theoretical background

3.1. Variational mode decomposition

VMD transmits the acquisition process of signal components and uses a non-recursive processing strategy to achieve the central frequency and bandwidth limitation to obtain the effective components and modal functions corresponding to each centre frequency in the frequency domain. In recent years, VMD has been used to solve many engineering problems, such as gravimeter signal denoising, vibration and shock signal analysis, mechanical fault diagnosis and *et al*, because of its ability to mine complex signal features.

The decomposition process of VMD mainly includes the construction and the solution of the variational problem, with two main constraints: (a) the sum of the bandwidth of the

centre frequencies of each modal component is the minimum; (b) the sum of all modal components is equal to the original signal. The original signal could be decomposed into individual intrinsic mode functions (IMF) components, which are defined as an AM-FM (amplitude–frequency modulation) signal. The expression of the first IMF is:

$$u_k(t) = A_k(t) \cos[\phi_k(t)], \quad k \in \{1, \dots, K\} \quad (7)$$

where the phase $\phi_k(t)$ is a non-decreasing function, and $\phi_k'(t)$ is not less than 0, $A_k(t)$ is the envelope function and slowly variable compared to the phase. The bandwidth of each IMF component can be estimated according to the Carson criterion:

$$\text{BW}_{\text{AM-FM}} = 2(\Delta f + f_{\text{FM}} + f_{\text{AM}}) \quad (8)$$

where Δf represents the maximum deviation of the instantaneous frequency from the centre, f_{FM} represents the offset rate of the instantaneous frequency, and f_{AM} represents the highest frequency of the envelope function $A_k(t)$. Under the constraint that the sum of each component is equal to the input signal, and the sum of the estimated bandwidth of each component is minimized. After transformation, the following constraint variational model is constructed by formula (9):

$$\begin{aligned} \min_{\{u_k\}, \{\omega_k\}} & \left\{ \sum \|\partial_t \left[\left(\delta(t) + \frac{j}{\pi t} \right) u_k(t) \right] e^{-j\omega_k t} \|^2 \right\} \\ \text{s.t.} & \sum_k u_k = x \end{aligned} \quad (9)$$

where $\{u_k\}$ represents the decomposed IMF component, $\{\omega_k\}$ represents the central frequency corresponding to the IMF component, $(\delta(t) + j/\pi t)u_k(t)$ represents the one-side spectrum of the IMF component obtained by the Hilbert transformation, and x is the original input signal. To solve this constrained variational model, a constrained variational problem is transformed into an unconstrained variational problem by introducing a second-order penalty factor and a Lagrange multiplier term with the formula (10).

Table 1. Principle of VMD algorithm.

Algorithm. Complete optimization of VMD.

Initialize $\{\hat{u}_k^1\}, \{\omega_k^1\}, \hat{\lambda}^1, n \leftarrow 0$

Repeat $n \leftarrow n + 1$

for $k = 1 : K$ do

Update \hat{u}_k for all $\omega \geq 0$:

$$\hat{u}_k^{n+1}(\omega) \leftarrow \frac{\hat{f}(\omega) - \sum_{i < k} \hat{u}_i^{n+1}(\omega) - \sum_{i > k} \hat{u}_i^n(\omega) + \frac{\hat{\lambda}^n(\omega)}{2}}{1 + 2\alpha(\omega - \omega_k^n)^2}$$

Update ω_k :

$$\omega_k^{n+1} \leftarrow \frac{\int_0^\infty \omega |\hat{u}_k^{n+1}(\omega)|^2 d\omega}{\int_0^\infty |\hat{u}_k^{n+1}(\omega)|^2 d\omega}$$

end for

Dual ascent for all $\omega \geq 0$:

$$\hat{\lambda}^{n+1}(\omega) \leftarrow \hat{\lambda}^n(\omega) + \tau(\hat{f}(\omega) - \sum_k \hat{u}_k^{n+1}(\omega))$$

until convergence: $\sum_k \|\hat{u}_k^{n+1} - \hat{u}_k^n\|_2^2 / \|\hat{u}_k^n\|_2^2 < \varepsilon$.

The point of the variational problem above is to update through alternation u_k^{n+1} , ω_k^{n+1} and λ^{n+1} , this process is listed in the above algorithm,

$$L(\{u_k\}, \{\omega_k\}, \lambda) = \alpha \sum_k \left\| \partial_t \left[(\delta(t) + \frac{j}{\pi t}) u_k(t) \right] e^{-j\omega_k t} \right\|_2^2 + \left\| f(t) - \sum_k u_k(t) \right\|_2^2 + \left\langle \lambda(t), f(t) - \sum_k u_k(t) \right\rangle. \quad (10)$$

According to the process of VMD and the correlation analysis in [6–8], when K is selected appropriately, VMD decomposes the frequency components contained in the original signal very well, but an improper selection of K will lead to under or over decomposition. Similarly, some frequency signals would be in the under-decomposed state or be incorrectly decomposed. When α is too small, the central frequency of each component is more accurate than if α is too large, but the number of iterations completed by decomposition increases rapidly. Therefore, it is necessary to design a method to accurately select K and α .

3.2. K–L divergence

K–L divergence, also known as relative entropy, could be used to determine the degree of likelihood of the occurrence of two probability distributions, equivalent to the information entropy difference of the two probability distributions, which is shown as formula (11), where $p(x_i)$ is the probability distribution of the real data, and $q(x_i)$ is the theoretical probability distribution. The relative entropy of the two groups of data close to each other is small, and that of the two groups of scattered data are large. This method could use a more superficial and approximate distribution to substitute for the observed data or too complex a distribution,

$$D_{KL}(p||q) = \sum_{i=1}^N p(x_i) \cdot (\log p(x_i) - \log q(x_i)). \quad (11)$$

The K–L divergence of each mode of VMD is iteratively summed in an ergodic manner, and the optimal K and α are obtained while the sum value is the smallest. For specific implementation, the initial value of α was given as 2000. For example, the initial value of the modal K was set as 2, with a maximum value of 20 and the step size of 1. In this case, K was obtained corresponding to the minimum value of the sum of K–L divergence, and then the α could be determined accordingly. This method is easy to execute, requires less computational time, is more convenient in code writing and data processing with simple operation logic, and has been designed for near real-time processing of satellite atomic clock signals.

3.3. Permutation entropy

The PE algorithm could reflect system complexity and be used to detect time series random term mutations with strong robustness; PE algorithms have been widely used in nonlinear

data processing and analysis [21]. To solve the PE of the i mode component, $IMF_i(t)$ of length N is reconstructed in m dimensional phase space to generate the IMF of $K \times m$:

$$IMF = \begin{bmatrix} IMF_i(1) & IMF_i(1+\tau) & \dots & IMF_i(1+(m-1)\tau) \\ IMF_i(2) & IMF_i(2+\tau) & \dots & IMF_i(2+(m-1)\tau) \\ \vdots & \vdots & \ddots & \vdots \\ IMF_i(K) & IMF_i(K+\tau) & \dots & IMF_i(K+(m-1)\tau) \end{bmatrix} \quad (12)$$

where each row of IMF is a reconstruction component, m is the dimension number, τ is the delay time, and K is equal to $N - (m - 1)\tau$ as well as no bigger than $m!$. Then, a set of symbols could be obtained for each row vector of the reconstructed matrix, which could be expressed as follows:

$$S(l) = \{j_1, j_2, \dots, j_m\}, \quad l = 1, 2, \dots, K. \quad (13)$$

The number of the symbolic sequence occurrence of each $S(l)$ is counted. Then, the probability P_l is calculated by dividing $S(l)$ by $m!$. The probability of occurrence of each symbol sequence is calculated as P_1, P_2, \dots, P_l . The PE of the modal component $IMF_i(n)$ can be expressed with the standard in the form of Shannon entropy as follows:

$$PE_i = - \sum_{l=1}^K P_l \ln(P_l). \quad (14)$$

Finally, the PE value of every IMF needs to be normalized based on the maximum PE of modal components. The entropy value indicates the degree of randomness, where a small value corresponds to simple and regular time series, and a large value represents complex and random time series. Thus, PE is introduced to qualitatively analyse the signal-dominant component and the noise-dominant component in the clock signal.

3.4. Savitzky–Golay (SG) filter

SG filter, a method proposed by Savitzky and Golay to eliminate noise based on a polynomial fit on the time domain, has been widely applied in denoising signals containing various irregular noises [22]. The main feature of this method is that the shape and width of the denoised signal remain unchanged. Thus effectively retaining the change information of the signal, which is vital for a satellite atomic clock’s signal. The filtering is realised by formula (15):

$$\min \sum_{j=-m}^m (Y_j - y_j)^2, \quad s.t. Y_l = c_0 + c_1 i + c_2 i^2 + \dots + c_p i^p. \quad (15)$$

4. Framework of a K–L VMD-PE-SG-based model

The present study proposed a VMD-PE-SG model based on K–L divergence to denoise the satellite atomic clock’s signal. The framework of the presented denoising method is illustrated in figure 1. Firstly, VMD was applied to

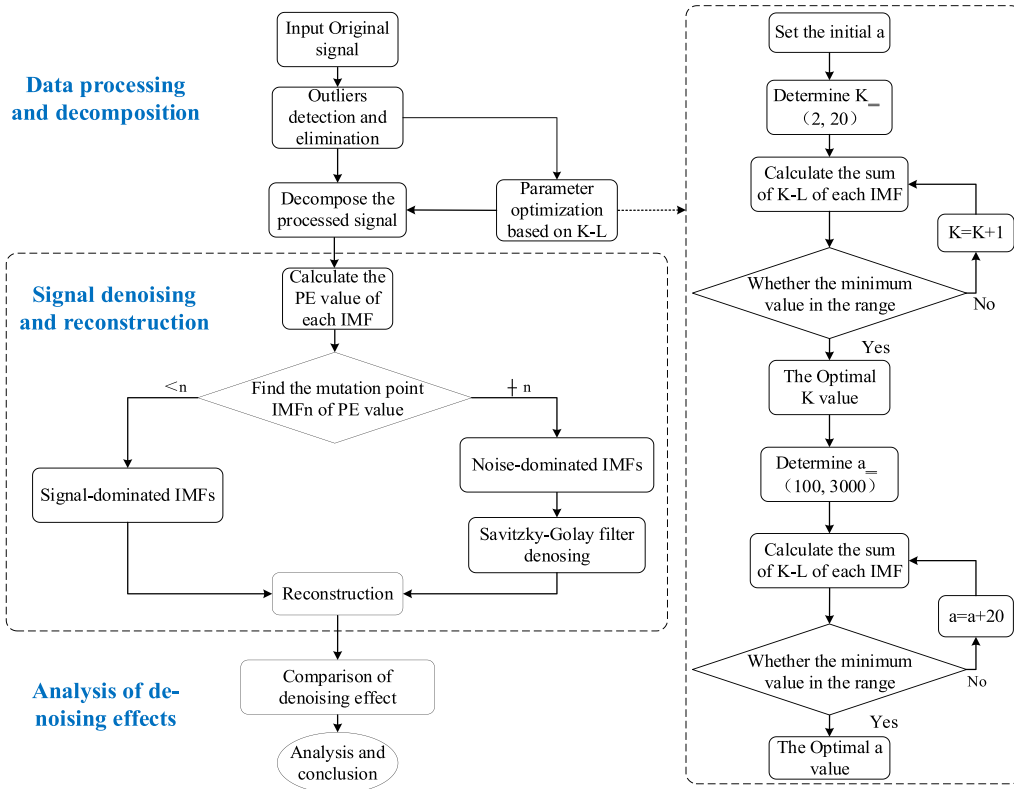


Figure 1. The flow chart of K–L VMD-PE-SG denoising for satellite atomic clock.

perform preliminary processing and decomposition of the measurement data of the satellite atomic clock. Secondly, the noise characteristics were determined according to the PE values of each decomposition mode, and the signal reconstruction was completed under SG filtering. Finally, the characteristics of the reconstructed signals were analysed, and the effectiveness of the method was verified. Based on the constraint of K–L divergence, the main parameters suitable for the VMD could be obtained. The optimised VMD decomposes the satellite clock signal with complex variation characteristics into a subseries with simple variation characteristics. The PE was introduced to help determine signal- or noise-dominated subsequences, and then the SG filter was used to process the noise components to avoid the loss of useful information. Finally, the denoised signal was reconstructed from the processed subsequences, and its impact was analysed. The specific steps of the algorithm can be expressed as figure 1.

Step 1: Perform the necessary processing of the satellite atomic clock data, including outlier detection and elimination based on the median value. Because the clock frequency bits are more effective than the phase, the satellite clock offset data is converted to the average frequency.

Step 2: Take the K–L divergence as the constraint condition. K and α are the optimal decomposition values at the minimum K–L sum value. Then the satellite clock’s signal is decomposed by VMD.

Step 3: Calculate the PE value of each IMF, the signal- and noise-dominated IMF are distinguished by the mutation point of PE of two adjacent IMF.

Step 4: Denoise the noise-dominated IMF by SG filter.

Step 5: Accumulate the signal-dominated IMF and the processed noise component to obtain the denoised signal.

5. Simulation

5.1. Simulation signal generation and time-frequency characteristic analysis

$$\begin{cases}
 y_1(t) = 6 \times 10^{-14} \times \sin(\pi t/43200 + \pi/5) \\
 y_2(t) = 1 \times 10^{-13} \times \cos(\pi t/14400 + \sin(\pi t/86400)) \\
 y_3(t) = 1 \times 10^{-13} \times (1 + 0.3 \times \cos(\pi t/10800)) \cdot \sin(\pi t/8640) \\
 y_4(t) = 1 \times 10^{-13} \times \text{wgn}(\text{length}(t), 1, 0) \\
 \text{Pure signal} = y_1(t) + y_2(t) + y_3(t) \\
 \text{Mixed signal} = y_1(t) + y_2(t) + y_3(t) + y_4(t)
 \end{cases} \quad (16)$$

The signal generated by a satellite atomic clock in space is very complex showing nonlinear and non-stationary characteristics. A frequency signal similar to the characteristics of the satellite atomic clock was modulated to verify the effectiveness of the proposed method. For a short-term atomic clock signal, let us assume that the deterministic components, including y_0 and d , are constants and not a key consideration. Thus, the simulation signal consists of sinusoidal signal $y_1(t)$ with a cycle of 86 400 s (24 h), frequency modulation signal $y_2(t)$ with the main cycle of 28 800 s (8 h), amplitude

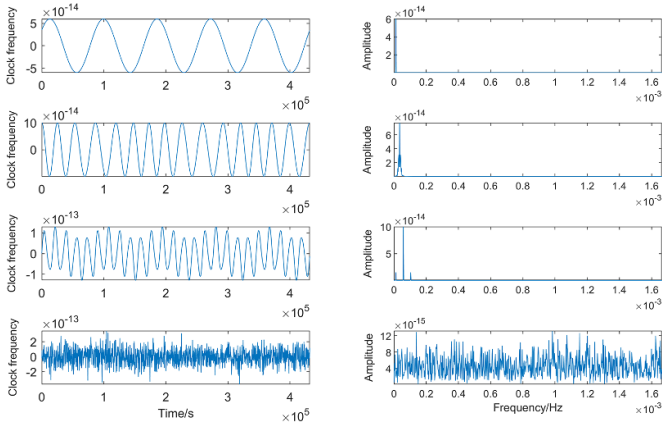


Figure 2. Time-frequency waveform of each sub-signal in the simulation signal.

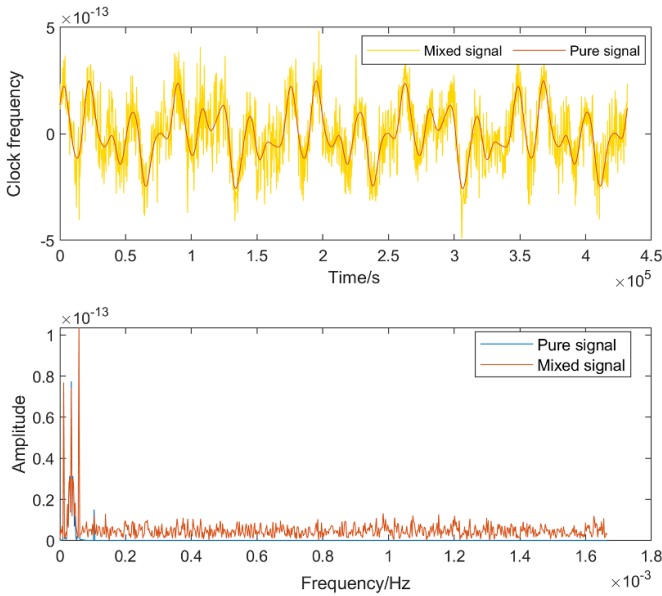
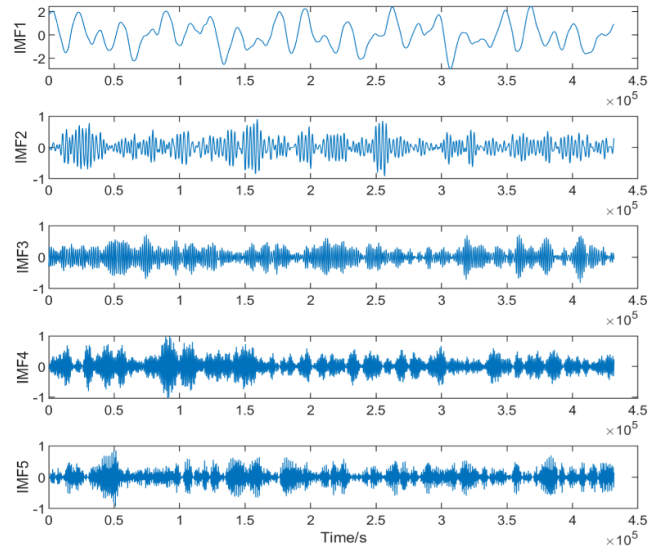


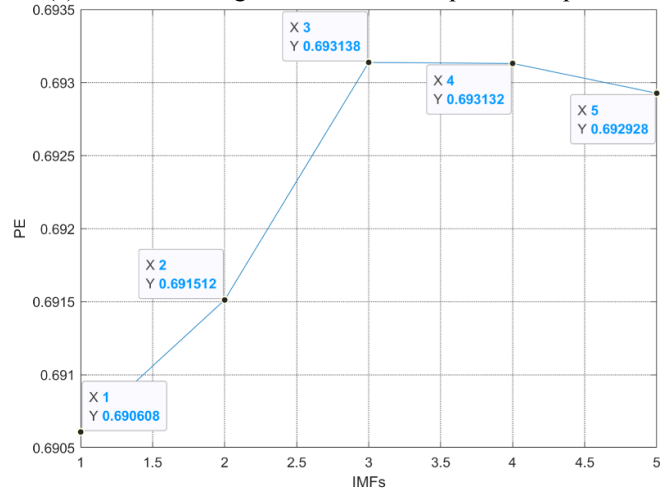
Figure 3. Time-frequency waveform of the pure and the mixed signal.

modulation signal $y_3(t)$ with the main cycle of 21 600 s (6 h), random noise $y_4(t)$ with an amplitude of 1×10^{-13} , a standard deviation of 1 and an intensity of 0 dB.

The time range was selected by $t = 0 : 300 : 1439 \times 300$ (five days) as an example. The corresponding time-frequency waveform of each sub-signal is shown in figure 2. This figure shows that the characteristics of each signal are quite different. The main periodic terms of the first three signals are apparent, but the waveforms of noise signals are chaotic and have no periodic characteristics. The waveforms of the pure signal and the mixed signal are shown in figure 3. It can be seen that with a large order of noise, the waveform of the mixed signal $y_4(t)$ almost masks the characteristics of the pure signal, and there are many chaotic components in the high-frequency part of the frequency domain waveform, which makes it difficult to analyse and deal with signals.



(a) Waveform diagram of each decomposed component



(b) PE of each decomposition component

Figure 4. Simulation signal waveform and its PE decomposed by VMD.

5.2. Analysis of the denoising effect of the simulation signal

In order to decompose the simulation signal with noise, the optimal values of K and α were obtained by K-L divergence, with the result of 5 and 2120, respectively, and importantly, the parameter optimization process took no more than 23.38 s. The experiment used a Windows 10 operating system, an Intel Core i5-11300H processor and the matlab2021a computer language for simulation. Based on the above parameters, the waveform diagram of each component of the simulation signal decomposed by VMD is shown in figure 4, and the corresponding PE values are also given.

Based on the PE of every IMF, the differences between two adjacent modes were calculated, resulting in 0.000 904, 0.001 626, 0.000 006, and 0.000 204 sequentially. It could be concluded that the sudden change of the PE appeared between the second adjacent modes, which means that the first two IMFs were signal-dominated components and the rest were noise-dominated components. Thus, an SG filter with

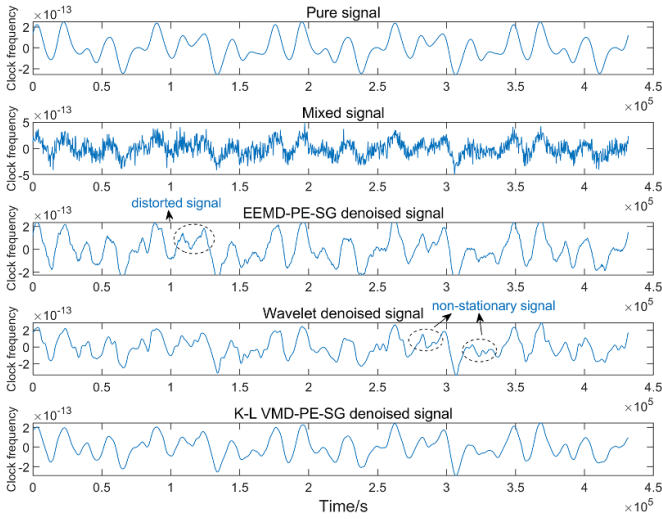


Figure 5. Denoising waveforms of various methods.

polynomial order 3 and data frame length 27 was applied to the mode IMF3–IMF5 and reconstructed into a denoised signal together with the first two modes. To verify the effectiveness and practicability of the K–L VMD-PE-SG method, wavelet denoising of Daubechies (db4) with good orthogonality and EEMD were selected as a comparison, where the components decomposed by EEMD were performed in the same way as the proposed algorithm. The denoising waveforms of various methods and original signal waveforms are given in figure 5, which shows that the waveform of the signal obtained by EEMD or wavelet denoising was improved compared with the mixed signal but still significantly different from the pure signal.

Some local distorted signals were generated after EEMD denoising, and non-stationary signals existed in the waveform of wavelet denoising, which indicated that the denoising performance of these two methods needs to be improved. In contrast, the denoised data of the proposed algorithm contained essentially no distortion and non-smoothed signals and was close to a pure signal waveform. In order to quantify the effectiveness of different methods, the signal-noise ratio (SNR) and root mean square (RMS) of the denoising method were calculated. The calculation method of the two indicators was calculated by formulas (17) and (18):

$$SNR = 10 \lg \frac{\sum_{i=1}^n x_i^2}{\sum_i (y_i - x_i)^2} \quad (17)$$

$$RMS = \sqrt{\frac{\sum_{i=1}^n (x_i - y_i)^2}{n}} \quad (18)$$

where x_i represents pure signal and y_i represents the signal processed by different methods; the SNR and RMS indices after denoising by different methods are shown in table 2. It can be seen that the SNR increased (considered an improvement)

Table 2. Characteristic values of different signals.

Methods	SNR (dB)	RMS ($\times 10^{-13}$)
Mixed signal	1.0971	1.0011
Wavelet	10.6259	0.3342
EEMD-PE-SG	11.3009	0.3092
The proposed method	13.6977	0.2346

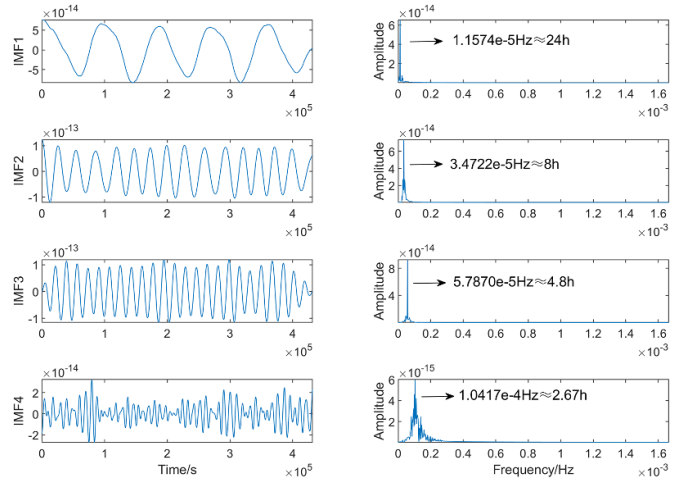


Figure 6. The time domain waveforms of the VMD of the denoised signal using the denoising method based on VMD.

and the RMS decreased after denoising, in which the denoising ability of EEMD-PE-SG was slightly better than that of wavelet denoising but still lower than that of the K–L VMD-PE-SG method. In terms of indicators, the SNR of the proposed method provided improved results when compared with EEMD-PE-SG and wavelet denoising by 21.2% and 28.9%, respectively, and RMS is improved by 24.1% and 29.8%, respectively.

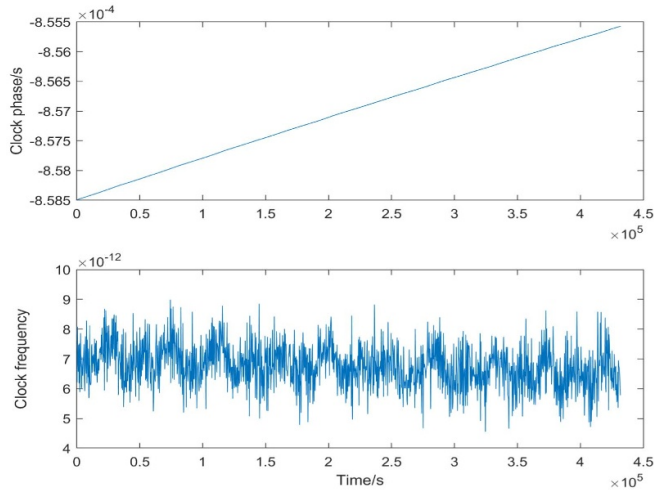
5.3. Analysis of the decomposition effect of the reconstructed signals

VMD has a great sensitivity to noise. After the noise reduction of a simulated signal, the proposed method was used to decompose the processed signal once more. Figure 6 shows the time domain waveform of each decomposed component and the corresponding spectrum diagram. Intuitively, the first three items decomposed are roughly consistent with the effective signal of the pure signal, and the last component is stable and regular. As a result, the proposed method can successfully separate the single component, and the decomposition accuracy and effect are improved after denoising.

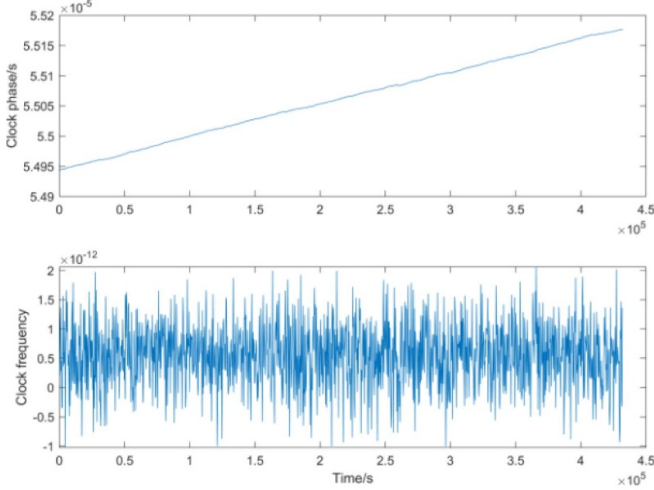
6. Denoising of the satellite atomic clock frequency

6.1. Experimental data

The experimental data were selected from the precise clock offset data of BDS and GLONASS satellites released by the GNSS Research Center of Wuhan University. The BDS-3



(a) The phase and frequency of the C37 clock



(b) The phase and frequency of the R01 clock

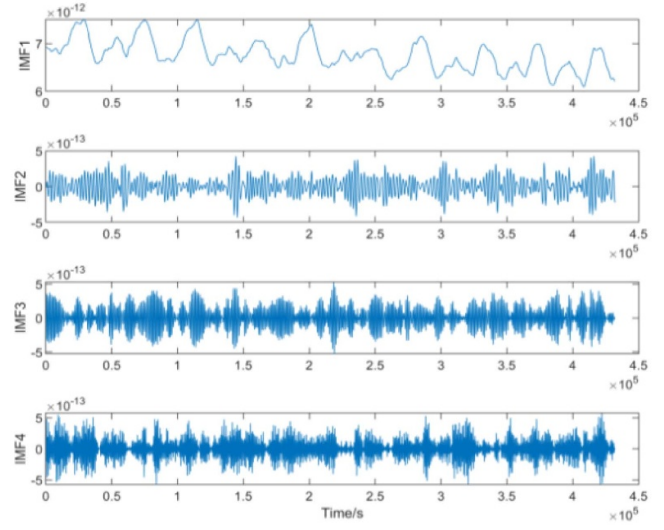
Figure 7. The phase and frequency for two selected clocks.

rubidium (Rb) clock numbered C37 with good data continuity, the most widely used clock in BDS, and a GLONASS-M caesium (Cs) clock numbered R01 were applied to the analysis. About 1440 data points acquired during five days from 4 July to 8 July 2021, were taken, and the epoch interval was 5 min.

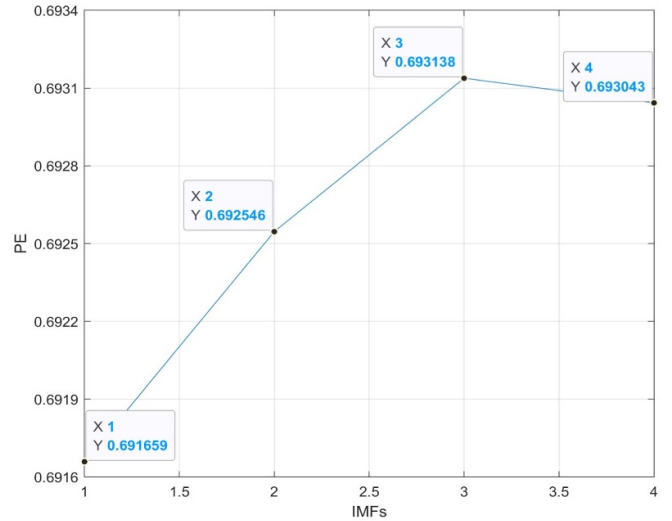
The selected satellite clock offset data and the corresponding average frequency data are shown in figure 7. They were processed by outliers detection based on median absolute deviation (MAD). As shown in figure 7, the order of magnitude of satellite clock phase data was quite large, so its non-stationary characteristics were difficult to observe. After conversion to the average frequency, it was easy to observe that the frequency has complex variation characteristics and a large amount of noise. Therefore, it is necessary to denoise the satellite atomic clock frequency data.

6.2. Implementation of denoising

First of all, the C37 satellite atomic clock is taken as an example to explain the denoising process step by step. Then, the stability results of the C37 and R01 satellite atomic clocks



(a) Waveform diagram of each decomposed component



(b) PE of each decomposition component

Figure 8. Clock signal waveform and its PE decomposed by VMD.

after denoising are given. Finally, the test phenomena are comprehensively discussed and analysed.

For the C37 clock, the VMD optimised by K-L divergence was applied to decompose the selected frequency data and the obtained four modes are shown in figure 8, whose corresponding PE was given together. Based on the PE of every IMF, the difference between two adjacent modes was calculated, resulting in 0.000 887, 0.000 592, and 0.000 095 sequentially. It could be concluded that a sudden change of the PE appeared between the first adjacent modes, which means that the first IMF were signal-dominated components and the rest were noise-dominated components. Thus, the SG filter with polynomial order 3 and data frame length 27 was applied to the mode IMF2-IMF4 and reconstructed into a denoised signal together with the first mode.

The satellite atomic clock frequency data waveform after denoising by the K-L VMD-PE-SG method is shown in figure 9, and the waveforms obtained by the two comparison methods are also given. It can be seen that although

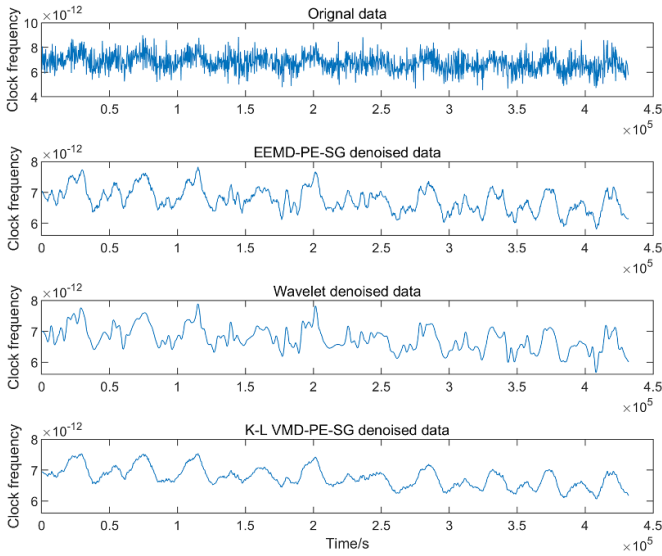


Figure 9. Denoising and original waveforms of experimental data.

the signal after EEMD and wavelet denoising was relatively regular compared with the original signal, it still showed the same problems as the simulated signal, including the local distortion and non-stationary characteristics. In contrast, the signal denoised by the proposed method was smoother, which could better reflect the law of frequency change.

6.3. Analysis of frequency stability

The experimental data were obtained by the ground laboratory, including calculating the satellite-ground comparison data, and the pure signal of the satellite atomic clock could not be available, so SNR and RMSE could not be used to quantify the effectiveness of the denoising method. For this reason, the performance of the proposed method was mainly tested through an analysis of frequency stability. Formula (19) was used to calculate the stability with the frequency data:

$$\sigma_y^2(\tau) = \frac{1}{2(M-1)} \sum_{i=1}^{M-1} (y_{i+1} - y_i)^2 \quad (19)$$

where τ is the sampling time, M is the number of the sampling frequency, and $\sigma_y(\tau)$ is ADEV, the most commonly used index to characterize frequency stability. The ADEV curves of the original signal and the signals denoised by different methods for C37 are shown in figure 10. It can be seen that the three methods could effectively improve the short-term frequency stability and suppress the influence of short-term dominant noise with a negative slope, and the proposed method had the best effect. When the smoothing time was about 10 000 s, due to the distortion caused by EEMD and wavelet denoising, the frequency stability of the two signals was even worse than that of the original signal.

The frequency stability values of different smoothing times are summarized in table 3 to quantify the denoising effect of relevant methods. It can be seen that the denoising effect of the wavelet and EEMD methods is limited, and the

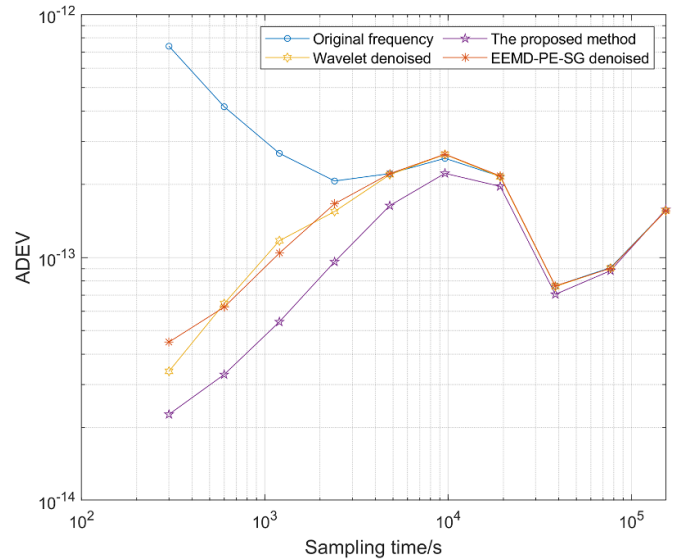


Figure 10. Frequency stability of C37 before and after denoising.

Table 3. Frequency stability of C37 obtained by different methods.

methods	ADEV ($\times 10^{-13}$)			
	Sampling time (s)			
	9600	19 200	38 400	76 800
Original signal	2.56	2.16	0.764	0.908
Wavelet	2.65	2.14	0.759	0.904
EEMD-SG-PE	2.66	2.15	0.763	0.903
The proposed method	2.21	1.96	0.705	0.883

proposed method can significantly improve the stability of each smoothing time. Specifically, in the smoothing times of 9600 s, 19 200 s, 38 400 s and 76 800 s, the frequency stability was 13.3%, 9.3%, 7.8% and 2.8% higher than that of the original data, respectively. It is worth noting that the denoising effect for C37 decreased over time, and when the time increased to more than one day, the stability of different models tended to be consistent, mainly because the contribution of frequency drift to the stability, which starts to dominate and gradually submerges the noise characteristics.

To illustrate the effectiveness of this method on different types of GNSS satellite clocks, and further analyse the influence of frequency drift on noise removal, the GLONASS R01 Cs clock with a tiny frequency offset was analysed. The ADEV curves of the original signal and the signals denoised by different methods for R01 are shown in figure 11. It can be seen that the three methods could effectively improve the short-medium term frequency stability and suppress the influence of short-medium term dominant noise with a negative slope, and the proposed method had the best effect.

The frequency stability values of different smoothing times are summarized in table 4 to quantify the denoising effect of each relevant method. It can be seen that the denoising effect of wavelet and EEMD methods is limited, and the proposed method can significantly improve the stability of each smoothing time. Specifically, with the smoothing times of 9600 s, 19 200 s, 38 400 s and 76 800 s, the frequency stability was

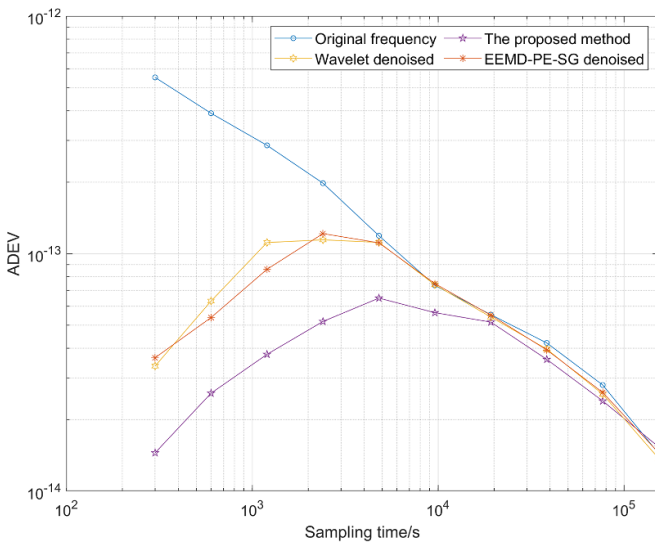


Figure 11. Frequency stability of R01 before and after denoising.

Table 4. Frequency stability of R01 obtained by different methods.

methods	ADEV ($\times 10^{-14}$)			
	Sampling time (s)			
	9600	19 200	38 400	76 800
Original signal	7.351	5.532	4.214	2.803
Wavelet	7.388	5.407	3.956	2.563
EEMD-SG-PE	7.467	5.501	3.928	2.601
The proposed method	5.640	5.143	3.576	2.387

23.3%, 7.1%, 14.9%, and 14.6% higher than the original data, respectively. Among these, the stability improvement amplitude was the smallest at the smoothing time of 19 200 s, reflecting the influence of the periodic term on the stability. The analysis results show that the proposed method is effective for Cs clocks, and its denoising effect is more significant than that of Rb clocks, which may be due to the inconspicuous drift characteristics.

7. Conclusion

This study analysed the influence of different components of satellite clock offset on frequency stability, the necessity of denoising clock difference data is expounded, and a denoising method of satellite clock offset signal based on K–L VMD-PE-SG is put forward. In the proposed method, K–L divergence is specifically applied to the parameter optimization of VMD, and PE is introduced to distinguish the noise of each sub-signal decomposed by VMD. In order to avoid the omission of useful information, the first item of VMD is not directly taken as the processed signal but reconstructed with the noise signal filtered by the SG filter to generate the denoising signal.

The results show that the proposed K–L VMD-PE-SG-based method achieves a better denoising effect than the EEMD and wavelet denoising methods. Compared with EEMD-PE-SG and wavelet denoising methods, the SNR of the proposed method was improved by 21.2% and 28.9%, and

the RMS is improved by 24.1% and 29.8%, respectively. The proposed denoising method fully combines the K–L divergence characteristics, thus providing accurate parameters for VMD in a short time, the useful information of satellite atomic clock signals can be completely retained through signal identification and reconstruction. As a result, the proposed method can significantly affect the dominant noise in the short term, such as WFM, to effectively improve the short-term frequency stability.

It is worth discussing that the denoising effect of the proposed method varies for different types of atomic clocks, which is mainly due to the different frequency drift characteristics of those clocks. The denoising ability of the proposed method also varies with smoothing time for the same satellite atomic clock due to the inclusion of periodic terms and drift components in the signal, which have time-varying effects on the frequency stability. In addition, improving the proposed method on the long-term frequency stability needs to be further verified, which is an essential work being planned.

In summary, the proposed method takes only a short time to complete the signal denoising of the clock and can give full play to its advantages in favour of short-medium term stability. Therefore, it has broad prospects in various applications, such as frequency and clock offset prediction atomic time algorithms.

Data availability statement

The data that support the findings of this study are available upon reasonable request from the authors.

Acknowledgments

The authors would like to acknowledge the Global Navigation Satellite System (GNSS) Research Centre of Wuhan University for providing the precise clock offset data on the China’s BeiDou Satellite Navigation System (BDS) and Russia’s Global Navigation Satellite System (GLONASS).

Funding

This work was supported by the National Natural Science Foundation of China (Grant Nos. 41804076 and 61503404).

ORCID iD

Liang Yifeng  <https://orcid.org/0000-0002-0049-3090>

References

- [1] Huang G W, Cui B B, Zhang Q, Fu W and Li P 2018 An improved predicted model for BDS ultra-rapid satellite clock offsets *Remote Sens.* **10** 60–78
- [2] Jiang M, Dong S and Wu W 2020 Research on time scale algorithm based on hydrogen masers *IEEE Instrum. Meas. Mag.* **23** 35–40
- [3] Rui W A N G et al 2020 Comparison among algorithms for international atomic time *Acta Metrol. Sin.* **41** 363–8

- [4] Lin S Y 2016 A paper clock prediction model for UTC(TL) *Proc. IEEE 2016 European Frequency and Time Forum (EFTF)* pp 152–5
- [5] Huang N E, Shen Z, Long S R, Wu M C, Shih H H, Zheng Q, Yen N C, Tung C C and Liu H H 1998 The empirical mode decomposition and the Hilbert spectrum for nonlinear and non-stationary time series analysis *Proc. R. Soc. A* **454** 903–95
- [6] SONG H, Dong S, Wenjun W U, Jiang M and Wang W 2018 Detecting an atomic clock frequency anomaly using an adaptive Kalman filter algorithm *Metrologia* **55** 350–9
- [7] ZHU J-M et al 2017 The denoise of the atomic clock frequency differences *Acta Metrol. Sin.* **38** 499–503
- [8] Song H J, Dong S W and Ruan J 2017 Atomic time algorithm based on predictable weighting and wavelet multi-scale threshold denoising 2017 *Joint Conf. Uropean Frequency and Time Forum and Ieee Int. Frequency Control Symp. (Eftf/ifc)* pp 381–4
- [9] Mostafa A I, Hamza G G and Zekry A 2019 Using EMD for smoothing atomic clock error in national time scale algorithm 2019 *7th Int. Japan-Africa Conf. on Electronics, Communications and Computations (JAC-ECC)* pp 88–91
- [10] Klionskiy D, Kupriyanov M and Kaplun D 2017 Signal denoising based on empirical mode decomposition *J. Vibroeng.* **19** 5560–70
- [11] Torres M E, Colominas M A, Schlotthauer G and Flandrin P 2011 A complete ensemble empirical mode decomposition with adaptive noise *IEEE Int. Conf. on Acoustics, Speech and Signal Processing (IEEE)* pp 4144–7
- [12] Dragomiretskiy K and Zosso D 2014 Variational mode decomposition *IEEE Trans. Signal Processing* **62** 531–44
- [13] Wang J X, Zhang Y L, Zhang F Y, Li W, Lv S, Jiang M and Jia L 2021 Accuracy-improved bearing fault diagnosis method based on AVMD theory and AWPSO-ELM model *Measurement* **181** 109666
- [14] Kumar A, Zhou Y Q and Xiang J W 2021 Optimization of VMD using kernel-based mutual information for the extraction of weak features to detect bearing defects *Measurement* **168** 108402
- [15] Song Y Q, Deng S C and Lu Y G 2019 Application of K value optimized VMD in bearing fault diagnosis *Meas. Control Technol.* **38** 117–21
- [16] Liang T, Lu H and Sun H 2021 Application of parameter optimized variational mode decomposition method in fault feature extraction of rolling bearing *Entropy* **23** 520
- [17] WU Y-W, Yang B, Xiao S-H and Wang M 2019 Atomic clock models and frequency stability analyses *Geomat. Inf. Sci. Wuhan Univ.* **44** 1226–32
- [18] Galleani L and Tavella P 2015 The dynamic Allan variance IV: characterization of atomic clock anomalies *IEEE Trans. Ultrason. Ferroelectr. Freq. Control* **62** 791–801
- [19] Zucca C and Tavella P 2005 The clock model and its relationship with the Allan and related variances *IEEE Trans. Ultrason. Ferroelectr. Freq. Control* **52** 289–96
- [20] Galleani L and Tavella P 2010 Time and Kalman filter *IEEE Control Syst. Mag.* **30** 44–65
- [21] Bandt C and Pompe B 2002 Permutation entropy: a natural complexity measure for time series *Phys. Rev. Lett.* **88** 174102
- [22] Yang H, Cheng Y X and Li G H 2021 A denoising method for ship radiated noise based on Spearman variational mode decomposition, spatial-dependence recurrence sample entropy, improved wavelet threshold denoising, and Savitzky-Golay filter *Alex. Eng. J.* **60** 3379–400